Hydrologic Regulation of Chemical Weathering and the Geologic Carbon Cycle

K. Maher[1]* and C. P. Chamberlain[2]

Earth's temperature is thought to be regulated by a negative feedback between atmospheric CO_2 levels and chemical weathering of silicate rocks that operates over million-year time scales. To explain variations in the strength of the weathering feedback, we present a model for silicate weathering that regulates climatic and tectonic forcing through hydrologic processes and imposes a thermodynamic limit on weathering fluxes, based on the physical and chemical properties of river basins. Climate regulation by silicate weathering is thus strongest when global topography is elevated, similar to the situation today, and lowest when global topography is more subdued, allowing planetary temperatures to vary depending on the global distribution of topography and mountain belts, even in the absence of appreciable changes in CO_2 degassing rates.

Despite substantial changes in solar luminosity, plate tectonics, and atmospheric composition, over billions of years temperatures on Earth have remained favorable for liquid water and, by extension, life (*1*). A requirement for maintaining such clement conditions is a chemical weathering process that converts atmospheric CO_2 and silicate rocks to alkalinity and divalent cations, which are then buried on the seafloor as carbonate minerals (*2*–*5*). Chemical weathering rates cannot be out of balance with the supply of CO_2 from volcanic and metamorphic sources for very long without catastrophic consequences (*6*). Fortunately, such imbalances have been infrequent. Yet, Earth's climate has varied between warm ice-free conditions and cold extensively glaciated states, suggesting a climate system with variable regulation. The stability of Earth's climate thus requires both a negative feedback between chemical weathering rates and temperature and a mechanism that allows the strength of the feedback, or extent of regulation, to vary (*7*). The strength of the feedback is dictated by the functional relationship between the weathering rate and climate, and when balanced against CO_2 degassing rates, determines planetary temperatures (*4*–*7*). Several processes could allow the strength of the feedback to vary (*8*–*12*), suggesting that the mechanisms underlying one of the most profound features in the sculpting of Earth's history remain unresolved.

We developed a mathematical framework that captures how the strength of the weathering feedback changes as a function of the tectonic regime (*13*). We linked the weathering rate per unit of area of continent to the interaction between runoff and tectonic processes. The two are linked by the balance between the time that water spends in the weathering zone (fluid travel time), which depends on runoff and flow path length, and the kinetics of mineral weathering, which are a function of composition, temperature, and erosion rate. The weathering flux to the oceans should be maximized when thermodynamic equilibrium between the dissolving and precipitating minerals is approached, resulting in a "thermodynamic limit" not included in previous models. Conversely, weathering fluxes are at a minimum when fluid travel times are short relative to the time required for weathering reactions to reach equilibrium (equilibrium time). In this formulation, weathering rates can increase more substantially in tectonically active than in inactive areas in response to changes in climate, as suggested by numerical models (*7*, *14*).

The proposed model combines two equations: (1) a solute transport equation that quantifies weathering-derived solute as a function of the mean fluid travel time in a catchment and (2) an equation that relates the supply of fresh rock from erosion to the downward propagation of a weathering front. We calculate the solute concentration (C) as a function of the Damköhler number (Da) (*15*). The Damköhler number is a dimensionless number that compares the mean fluid travel time [$T_f \approx L\phi/q$(year)] to the time required to reach equilibrium [$T_{eq} \approx C_{eq}/R_n$(year)], where q[m/year] is runoff, the reactive flowpath length ($L\phi$) is flowpath length [L(m)] times effective porosity (ϕ), C_{eq}(μmol/liter) is the "thermodynamic limit" (i.e., the maximum concentration), and R_n(μmol/liter/year) is the reaction rate (n, a specific mineral composition) (*16*). Because runoff is a key variable, we factor out runoff and introduce the Damköhler coefficient (Dw), which is modified to account for the supply of fresh minerals through erosion.

$$Dw(\mathrm{m/year}) = \frac{L\phi}{T_{eq}} = \frac{L\phi R_{n,\max} f_w}{C_{eq}} \quad (1)$$

where the fraction of fresh minerals, f_w (= X_s/X_r), decreases with increasing soil age (T_s) or decreasing mineral supply rate (*17*–*20*) to moderate the maximum reaction rate ($R_{n,\max}$). The minimum T_{eq} occurs when the concentration of soil minerals (X_s) is equal to that of the original rock (X_r), or when T_s is very small, according to the

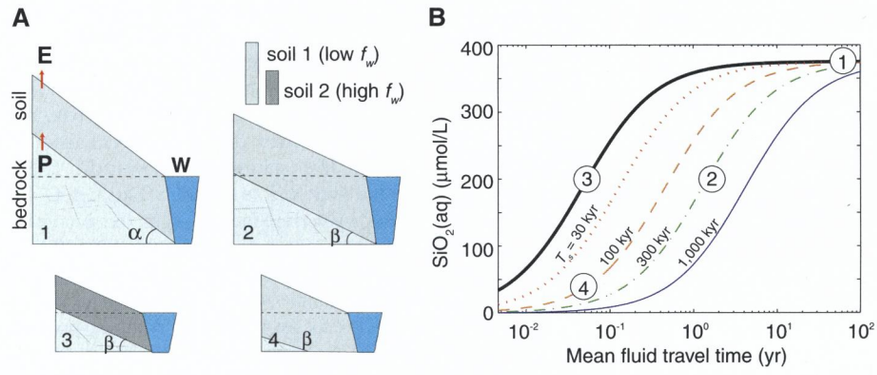

Fig. 1. Conceptual model for solute production in catchments. (**A**) Hillslope cross-sections with variable slope, soil thickness, mineral abundance, and mean fluid travel time. Red arrows show the production of soil from bedrock (*P*) and soil removal by erosion (*E*) and chemical denudation (*W*). Dashed lines indicate the water table, whereas slope is distinguished by angles α and β, with α > β. Soil thickness and f_w are equivalent for hillslopes 1, 2, and 4, whereas soil thickness is lower and f_w higher for hillslope 3. Fresh bedrock above the water table decreases the T_{eq}, so that $T_f > T_{eq}$. (**B**) Evolution of SiO_2(aq) as a function of T_f and T_s. The solid black line corresponds to weathering of fresh mineral, whereas light and stippled lines correspond to solute evolution for different T_s values. kyr, thousand years. Hillslope 1 (point 1) indicates a system at the thermodynamic limit where $T_f > T_{eq}$, as compared to hillslopes 2 to 4, where $T_f < T_{eq}$. Hillslopes 3 and 4 show how mineral supply (or f_w) affects solute production, hillslopes 2 and 4 show how T_f affects solute production, and the greater relief of hillslope 1 as compared to that of 2 results in larger $L\phi$.

[1]Department of Geological and Environmental Sciences, Stanford University, Stanford, CA 94305, USA. [2]Department of Environmental Earth System Science, Stanford University, Stanford, CA 94305, USA.

*Corresponding author. E-mail: kmaher@stanford.edu

following expression that is applicable to both steady-state (i.e., a balance between denudation and material supply) and transient landscapes

$$f_w(g/g) = \frac{X_s}{X_r} = \frac{1}{1 + mk_{eff}AT_s} \quad (2)$$

where k_{eff} is the weathering rate constant, A is the specific surface area of the minerals, and m is the molar mass of the weathering minerals [(*13*), table S1]. At a given runoff, larger Dw values reflect more-efficient solute generation and systems that are closer to the thermodynamic limit. The final equation for solute production is

$$C(\mu mol/L) = C_{eq}\frac{\tau Dw/q}{1 + \tau Dw/q} \quad (3)$$

where τ is a constant ($= e^2$) [(*13*), figs. S1 to S3]. The weathering flux (W) is computed from Eq. (3) as $C \times q$. Although we use SiO_2(aq) as a proxy for weathering, Ca and Mg derived from silicate weathering would show the same behavior (*13*, *16*). The solute production model does not capture all possible biogeochemical and climatic feedbacks that might operate on q, C_{eq}, k_{eff}, and T_s (*3*–*6*, *11*). Some key parameters are also not well constrained by observations, and hence our assumptions require further evaluation as suitable data become available (*21*).

The maximum solute concentration occurs when the mean fluid travel time (T_f) exceeds the equilibrium time (T_{eq}) at a given runoff. For example, consider a region on Earth at point 4 on Fig. 1, with short T_f and long T_{eq} (*22*). If fresh minerals are supplied to the weathering zone, T_{eq} decreases and solute concentrations increase, even with no change in T_f (point 3). As erosion increases and T_{eq} becomes less than T_f, the thermodynamic limit is approached (point 1) and solute concentration remains fixed. At the thermodynamic limit, concentration does not vary with runoff, as observed for some rivers (*23*, *24*). As declining surface uplift or erosion decreases the supply of fresh minerals from soil production, T_{eq} will increase, resulting in lower solute concentration, even if T_f remains long (point 2). Hence, climate (through runoff) is mechanistically coupled to erosion through the operative physical length scales and thermodynamic limits.

This formulation requires that as T_f becomes shorter than T_{eq}, solute concentrations decrease and solute fluxes plateau (Fig. 2). The Dw determines the runoff at which this plateau is reached. This relationship is observed in modern rivers draining active mountain ranges where high erosion and a rapid supply of fresh minerals result in short T_{eq}, so that solute concentrations and fluxes are high (Fig. 2). These systems have Dw values greater than 0.03 m/year. In contrast, in tectonically inactive areas, such as large cratons, the solute concentrations and fluxes are smaller and Dw values lower, because the reduced supply of fresh minerals to the weathering zone increases T_{eq} (*25*). The competition between T_f and T_{eq} in modern river basins is evident by the large range of Dw values—about a factor of 100. Although we use SiO_2(aq) as a proxy for weathering, Ca and Mg derived from silicate weathering would show the same behavior (*16*).

To change solute fluxes in rivers requires altering $L\phi$, T_{eq}, and/or runoff via tectonic and/or climatic events. For example, the construction of a mountain belt will alter all three of these parameters through the development of relief, an increased supply of fresh minerals (*26*, *27*), and increased runoff due to orographically induced precipitation (*28*). During initial mountain building, fresh rock exposed to the weathering zone shortens T_{eq} and increases solute concentrations (Fig. 3A). When mountains reach sufficient height to create orographic rainfall, solute fluxes will increase further with additional runoff. Even if thin soils result in short T_f in upland areas, the creation of upland topography may result in the deposition of reactive floodplains (*29*, *30*), a decrease in T_{eq}, and possibly an increase in T_f. Once the mountain belt reaches a physical steady state, no additional increase in chemical weathering is possible without a change in runoff. Finally, as tectonism wanes, reducing mineral supply to the weathering zone, solute fluxes decrease and complete the cycle.

The atmospheric heat budget of Earth is driven by the fluxes of atmospheric greenhouse gases, primarily CO_2. Silicate weathering is the dominant mechanism that sequesters CO_2 over geologic time scales (*2*). We propose that the removal of CO_2 is regulated by the intensity of the hydrologic cycle, rather than directly by temperature. Increases in global mean temperatures (GMTs) are associated with more precipitation and attendant changes in runoff (*31*), although climate model predictions vary widely. A climate model study of the response of runoff to increased GMT found an increase in runoff of 6.8 to 2.3%/°C between high- and low-latitude rivers, respectively (*31*). Because the effects of global warming on runoff will not be distributed evenly across latitudes, we use the maximum runoff sensitivity of 6.8%/°C GMT, so that a doubling of

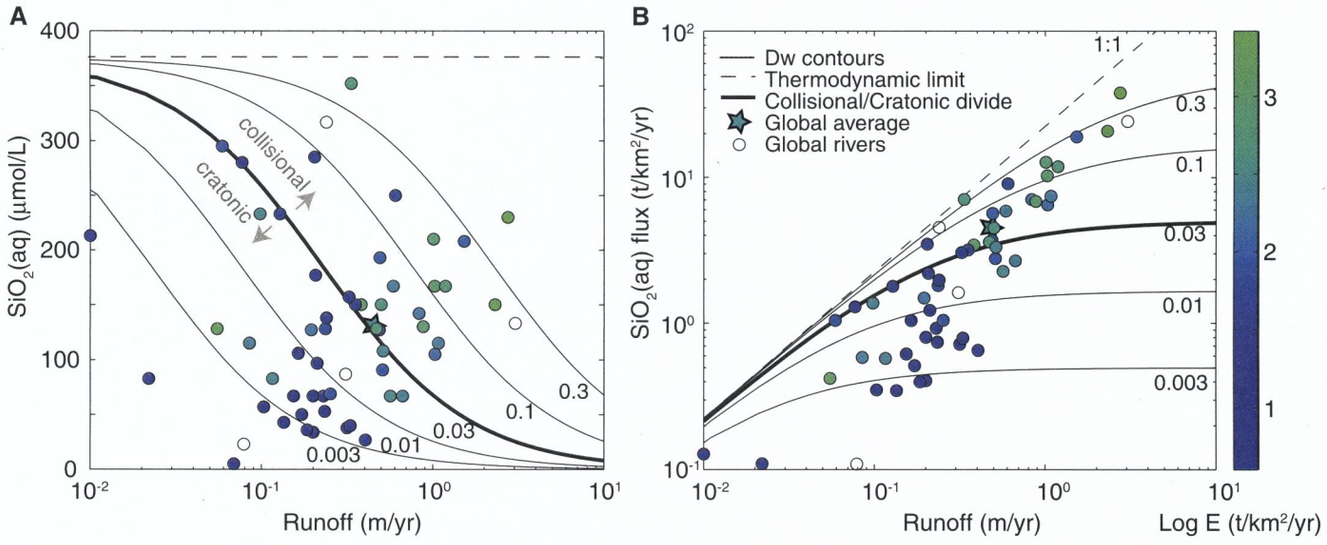

Fig. 2. Contours of global Damköhler coefficients applied to large rivers. (**A**) SiO_2(aq) for global rivers (*8*) as a function of runoff, compared to contours of Dw coefficients from 0.3 and 0.001 m/year, where 0.3 m/year corresponds to the global maximum Dw and C_{eq}. (**B**) SiO_2(aq) fluxes. The range of Dw contours corresponds to either changes in T_s from 0 to 1 million years, $L\phi$ of 0.10 to 0.001 m, or variations in both. A Dw of 0.03 m/year (collisional/craton divide) corresponds to $L\phi$ of 0.1 m and T_s of 100,000 years. The 1:1 line for flux:discharge is the thermodynamic limit. Each river is shaded according to the erosional flux (assumed to reflect mineral supply to the weathering zone), using the total suspended sediment flux.

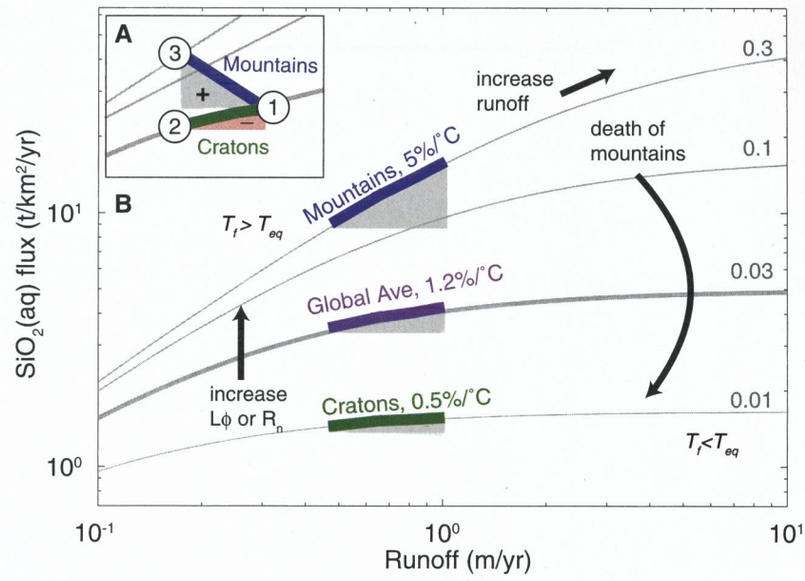

Fig. 3. Sensitivity of weathering fluxes to changes in GMT. (A) The inset depicts how an enhanced supply of fresh mineral from increasing erosion, combined with global cooling and decreased runoff, results in a decrease in weathering fluxes from the cratons (points 1 to 2, minus sign, pink wedge), whereas solute fluxes increase in mountains (points 1 to 3, plus sign, gray wedge), so that weathering fluxes (and global CO_2 levels) could remain at near-modern levels, depending on the area occupied by different weathering regimes. **(B)** Colored bars and gray wedges show the change in solute flux for a doubling of runoff for mountainous regions (blue), the global average (purple), and cratons (green), with the corresponding percent change in solute flux per °C of increase. Gray lines are contours of *Dw* as in Fig. 2.

runoff occurs with a temperature increase of 15°C. Assuming that temperature affects only runoff (supplementary text and figs. S7 and S8), changes in solute fluxes for a doubling of runoff across low-relief regions, active tectonic regions, and the global average indicate the differential climate sensitivity (Fig. 3B). Weathering fluxes in basins with moderate erosion rates, which represent a large portion of Earth's surface today (*32*), show minimal change. In contrast, active high-relief regions near the thermodynamic limit are the most sensitive to climatic changes (*27*), because higher *Dw* values afford a large change in runoff before maximum solute flux is achieved.

The order-of-magnitude difference in climate sensitivity between inactive and active tectonic regions may dramatically alter the global weathering feedback. The climate-weathering feedback is strongest in rapidly eroding regions near the thermodynamic limit, as shown by the wedges in Fig. 3B. In low-relief areas, the climate feedback is weaker, because solute fluxes plateau when T_{eq} exceeds T_f. During times of global warming and amplification of the hydrologic cycle, weathering fluxes will increase disproportionately between tectonically active and inactive areas, with high-relief tectonic areas providing proportionally more alkalinity to the oceans. At a given CO_2 degassing rate, global temperature is thus determined by the differential sensitivity of mountainous and low-relief areas to runoff, and will vary depending on the distribution of erosional regimes and mountain belts (Fig. 3A). This feature of our model allows weathering rates and atmospheric CO_2 to stabilize at different levels but prevents runaway CO_2 consumption during active tectonic periods, due to the enhanced climate sensitivity. Similarly, periods of warming and the attendant increases in runoff will drive weathering rates upward, particularly in mountainous regions. The solute production model explains the observed correlation between erosion and chemical weathering fluxes (*8*, *26*), while preserving the negative feedback between silicate weathering rates and global temperature.

References and Notes

1. C. Sagan, G. Mullen, *Science* **177**, 52–56 (1972).
2. J. C. G. Walker, P. B. Hays, J. F. Kasting, *J. Geophys. Res.* **86**, 9776 (1981).
3. R. A. Berner, Z. Kothavala, *Am. J. Sci.* **301**, 182–204 (2001).
4. R. A. Berner, A. C. Lasaga, R. M. Garrels, *Am. J. Sci.* **283**, 641–683 (1983).
5. L. R. Kump, S. L. Brantley, M. A. Arthur, *Annu. Rev. Earth Planet. Sci.* **28**, 611–667 (2000).
6. R. A. Berner, K. Caldeira, *Geology* **25**, 955 (1997).
7. L. R. Kump, M. A. Arthur, in *Tectonics Uplift and Climate Change*, W. F. Ruddiman, Ed. (Plenum, New York, 1997), pp. 399–426.
8. J. Gaillardet, B. Dupre, P. Louvat, C. J. Allegre, *Chem. Geol.* **159**, 3–30 (1999).
9. J. K. Willenbring, F. von Blanckenburg, *Nature* **465**, 211–214 (2010).
10. J. M. Edmond, Y. S. Huh, in *Tectonics Uplift and Climate Change*, W. F. Ruddiman, Ed. (Plenum, New York, 1997), pp. 329–351.
11. M. Pagani, K. Caldeira, R. Berner, D. J. Beerling, *Nature* **460**, 85–88 (2009).
12. S. E. McCauley, D. J. DePaolo, in *Global Tectonics and Climate Change*, W. F. Ruddiman, W. Prell, Eds. (Plenum, New York, 1997), pp. 427–467.
13. Methods and a complete description of the model are available on *Science* Online.
14. G. Li, H. Elderfield, *Geochim. Cosmochim. Acta* **103**, 11–25 (2013).
15. D. F. Boucher, G. E. Alves, *Chem. Eng. Prog.* **55**, 55 (1959).
16. K. Maher, *Earth Planet. Sci. Lett.* **312**, 48–58 (2011).
17. K. Yoo, S. M. Mudd, *Geology* **36**, 35 (2008).
18. G. E. Hilley, C. P. Chamberlain, S. Moon, S. Porder, S. D. Willett, *Earth Planet. Sci. Lett.* **293**, 191–199 (2010).
19. K. L. Ferrier, J. W. Kirchner, *Earth Planet. Sci. Lett.* **272**, 591–599 (2008).
20. S. Brantley, M. I. Lebedeva, *Annu. Rev. Earth Planet. Sci.* **39**, 387–416 (2011).
21. Independent calculation of *Dw* coefficients via Eq. 1 would be one approach. At present, sufficient data for large rivers are not available.
22. To compute the curves in Figs. 1 to 3, we use the concentration and discharge data of (*8*), $R_{n,max}$ of 1085 μmol SiO_2/liter/year, and a maximum C_{eq} of 375 μmol/liter (table S1) to determine the fluxes and *Dw* contours associated with the global rivers, mostly draining granitic lithologies. Basaltic lithologies are expected to follow the same general behavior (fig. S8). In Fig. 1, we show contours of T_s corresponding to *Dw* contours in Figs. 2 and 3. The contours of *Dw*, which do not depend on the absolute values of R_n, f_w, or T_s, illustrate how rivers respond in a relative sense to climatic and tectonic variations.
23. G. J. S. Bluth, L. R. Kump, *Geochim. Cosmochim. Acta* **58**, 2341–2359 (1994).
24. S. E. Godsey, J. W. Kirchner, D. W. Clow, *Hydrol. Processes* **23**, 1844–1864 (2009).
25. R. F. Stallard, J. M. Edmond, *J. Geophys. Res.* **88**, 9671 (1983).
26. M. E. Raymo, W. F. Ruddiman, *Nature* **359**, 117–122 (1992).
27. A. J. West, *Geology* **40**, 811–814 (2012).
28. S. D. Willett, *J. Geophys. Res.* **104**, 28957 (1999).
29. A. J. West, M. J. Bickle, R. Collins, J. Brasington, *Geology* **30**, 355 (2002).
30. J. Bouchez *et al.*, *Chem. Geol.* **332–333**, 166–184 (2012).
31. S. Manabe, R. T. Wetherald, P. C. D. Milly, T. L. Delworth, R. J. Stouffer, *Clim. Change* **64**, 59–76 (2004).
32. D. R. Montgomery, M. T. Brandon, *Earth Planet. Sci. Lett.* **201**, 481–489 (2002).

Acknowledgments: The paper benefitted greatly from the reviews provided by several anonymous reviewers. This work was supported by the U.S. NSF (EAR-1254156 to K.M.). Data used in this study come from previously published studies, and the details of the model are provided in the supplementary materials.

Supplementary Materials

www.sciencemag.org/content/343/6178/1502/suppl/DC1
Materials and Methods
Supplementary Text
Figs. S1 to S8
Table S1
References (*33–92*)

13 January 2014; accepted 25 February 2014
Published online 13 March 2014;
10.1126/science.1250770